NJC

ROYAL SOCIETY OF CHEMISTRY

PAPER

Cite this: *New J. Chem.*, 2023, **47**, 5667

Synthesis, characterization, and biophysical interaction studies of water-dispersible polypyrrole/polythiophene co-oligomers with bovine serum albumin and human serum albumin: an experimental and theoretical approach†

Ufana Riaz, *[ab] Aaliyah Farooq,[b] Nuzhat Nabi,[b] Faith R Nwanze[a] and Fei Yan[a]

Received 25th November 2022,
Accepted 8th February 2023

DOI: 10.1039/d2nj05791c

rsc.li/njc

The present work reports the synthesis of water-dispersible polypyrrole (WD-PPy) and polythiophene (WD-PTh) copolymers in different weight ratios and their characterization using experimental and theoretical techniques. The copolymers were spectroscopically characterized using experimental ^{13}C-NMR, FTIR, and UV-visible studies, and theoretical FTIR and UV-visible studies. The theoretical frequency and UV-visible data were computed using Gaussian 09 software with the functional DFT/B3LYP method and 6-31G(d) basis set. For the first time, biophysical interaction studies were carried out using bovine serum albumin (BSA) and human serum albumin (HSA) for these polymers which are not yet reported in the literature. The results showed strong binding of the co-oligomers with BSA/HSA which could be utilized in designing potent inhibitors and biosensors.

Introduction

Electroactive polymers such as polyaniline (PANI),[1] polypyrrole (PPy),[2] polythiophene (PTh),[3] poly(*o*-phenylenediamine) (POPD),[4] poly(1-naphthylamine) (PNA),[5] and polycarbazole (PCz)[6] have been utilized in diverse applications such as biosensors,[7] supercapacitors,[8] battery electrodes,[9] photocatalysts,[10] microbial fuel cells,[11] *etc.* Among them, PPy and PTh display exceptional properties such as ease of preparation, good redox behavior, high electrical conductivity, and good thermal stability.[12,13] The achievement of high conductivity is mainly due to the positive charge generated on the backbone of these polymers, particularly when polymerized using $FeCl_3$ as an oxidant which also acts as a dopant anion. However, most of the chemical and electrochemical techniques used for polymerization lead to the production of insoluble and intractable forms.[14,15]

Chemical polymerization is a facile technique to synthesize water soluble conducting polymers *via* the incorporation of flexible side chains which can solubilize in organic solvents. *Masuda and Kaeriyanma*[16] reported the synthesis of water-soluble conducting polymers using sodium salt of poly(thiophene-3-carboxylate). *Lu et al.*[17] reported the synthesis of PPy by interfacial polymerization at the interface of chloroform (with monomer) and water (with dopant/oxidizing agent) solutions. *Heeger et al.*[18] reported the synthesis of the sodium salts and corresponding acids of poly(thiophene ethane sulfonate) and poly(thiophene butane sulfonate). Wang and coworkers[19] synthesized a water-soluble polythiophene derivative with tyrosine kinase inhibitor *lapatinib* as a pendant moiety, used for imaging living cells.

The water solubility of conducting polymers provides a versatile platform for sensing various chemical and biological species due to the unique light-harvesting ability of these polymers. Fluorescence imaging and real-time sensing capacities demonstrate rapid and highly sensitive detection of various proteins such as bovine serum albumin (BSA) and human serum albumin *via* selective binding which are used to diagnose diseases/formulate several kinds of drugs. The ability of conducting polymers to act as a platform for protein–surface interactions and to covalently attach functional groups that provide protein binding sites has recently found immense application in the area of biosensors and for controlled cellular interactions.[20]

Keeping this in mind, we have developed water-dispersible PPy (WD-PPy), water-dispersible PTh (WD-PTh), and a series of copolymers of WD-PPy/WD-PTh *via* the interfacial polymerization method using different loadings of the monomers.

[a] *Department of Chemistry and Biochemistry, North Carolina Central University, NC, 27707, USA*
[b] *Materials Research Laboratory, Department of Chemistry, Jamia Millia Islamia, New Delhi 110025, India. E-mail: ufana2002@yahoo.co.in; Fax: + 91-112-684-0229*

† Electronic supplementary information (ESI) available: ^{1}H-NMR,^{13}C-NMR and IR spectra of PPy and PTh and their co-oligomers, and solubility data of oligomers and co-oligomers. See DOI: https://doi.org/10.1039/d2nj05791c

Interfacial polymerization has been used by authors to develop water-dispersible conducting polymers.[21,22] The homo-oligomers and co-oligomers revealed high water solubility and were characterized using ^{1}H-NMR ^{13}C-NMR, FTIR, UV-visible, and SEM analyses. The theoretical studies of these polymers were also computed *via* Gaussian 09 software using the B3LYP functional and 6-31G(d) basis sets. BSA and HSA were used as model proteins to explore the protein–polymer interactions due to their structural similarity, low cost, ease of purification, and ability to produce fluorescence emission. The interactions were investigated by UV-visible and docking studies.

Experimental

Pyrrole (Sigma Aldrich, USA), thiophene (Sigma Aldrich, USA), ferric chloride (Merck, India), dimethyl sulphoxide (DMSO) (Merck, India), and deionized distilled water were used without further purification.

Synthesis of water dispersible polypyrrole (WD-PPy)

A mixture of distilled water (40 ml) and DMSO (10 ml) was taken in a round bottom flask and the pyrrole monomer (8 ml, 0.11 mol) was added to the above mixture which was subjected to sonication in an ultrasonic bath at 30 °C equipped with a thermometer and nitrogen inlet. The mixing was carried out for around 2 h. $FeCl_3$ (3 g, 0.01 mol) was then added dropwise to the above solution and the color of the solution turned black indicating the onset of polymerization. The polymerization was allowed to continue for 24 h at 30 °C. The black precipitates obtained were filtered and washed with H_2O and ethanol to remove the traces of the oxidant from the synthesized product. The precipitate was dried in a vacuum oven at 60 °C for 24 h.

Synthesis of water dispersible polythiophene (WD-PTh)

The thiophene monomer (8 ml, 0.09 mol) was dissolved in chloroform (50 ml) in a 250 ml conical flask and was sonicated in an ultrasonic bath for about 4 h. $FeCl_3$ (3 g, 0.01 mol) dissolved in water (10 Ml) was then added dropwise to the thiophene solution and the mixture was sonicated for 24 h at 30 °C. The obtained precipitate of the polymer was filtered and washed with deionized water to remove the unreacted monomer, traces of the oxidant and other impurities. The filtrate was finally dried in a vacuum oven at 60 °C for 24 h.

Synthesis of water dispersible pyrrole/thiophene copolymers (WD-PPy/PTh)

Deionized distilled water (30 ml), DMSO (10 ml) and chloroform ((10 ml) in a 250 ml conical flask and a monomer of pyrrole (4 ml, 0.05 mol) and thiophene (4 ml, 0.05 mol) were added and sonicated in an ultrasonic bath for 4 h. $FeCl_3$ (3g, 0.01 mol) was added dropwise to the mixture of pyrrole/thiophene solution and sonicated for 24 h at 30 °C in the ultrasonic bath. The obtained copolymers were then filtered and washed with deionized water and ethanol to remove the unreacted monomer, oxidant and other impurities. The filtrate was finally dried in a vacuum oven at 80 °C for 24 h. The copolymer was designated as WD-PPy/PTh-1/1. A similar procedure was adopted for the synthesis of WD-PPy/PTh taking the mol ratios to be 4 : 1 and 1 : 4 which were designated as WD-PPy/PTh-4/1 and WD-PPy/PTh-1/4. The viscosity average molar mass of the synthesized polymers was determined as per the method reported in our earlier studies and was computed to be 3587 for WD-PPy, 4523 for WD-PTh, 5438 for WD-PPy/PTh-4/1, 4898 for WD-PPy/PTh-1/1 and 5804 WD-PPy/PTh-1/4.[23] Hence the polymers were designated as oligomers and co-oligomers.

Characterization

Spectral studies

The IR spectra of the co-oligomers were recorded using an FT-IR spectrophotometer model IRA Affinity-1 in the form of KBr pellets. UV-Vis spectra were recorded on a UV-Vis spectrophotometer model Shimadzu UV-1800 using water as a solvent. UV measurements were recorded using optical path lengths ranging between 1.0 and 10^{-2} cm for solutions. ^{1}H-NMR spectra were recorded at 25 °C on a Bruker 300 MHz spectrometer using deuterated dimethyl sulphoxide (DMSO) as a solvent. A fresh homogeneous solution was prepared using 50 mg of the oligomers in 0.5 ml of DMSO. The solutions were spiked with trimethylsilane (TMS) and analyzed in sealed 5 mm quartz NMR tubes with a spin speed of 20 Hz.

Gaussian calculations

The geometries were optimized at the B3LYP functional level using a 6-31G(d) basis set.[23] The oscillator strength, highest occupied molecular orbital (HOMO) and lowest unoccupied molecular orbital (LUMO) energies, and band gap were determined using the optimized geometries with the same basis set. The vibrational frequencies were computed using the same basis set. The UV spectra of optimized geometric structures were simulated at TD-DFT/B3LYP using the 6-31G(d) basis set.[23]

Biophysical interaction studies

The interaction of synthesized water dispersible polymers with bovine serum albumin (BSA) and human serum albumin (HSA) was studied *via* Uv–vis spectroscopy in buffer solution to explore the change in absorbance of the biological macromolecules upon interaction with polymers as per the method reported in our earlier studies.[24] The quantitative binding affinity of was analyzed using the Benesi–Hildebrand equation as mentioned in the literature.[25]

Docking studies

Molecular docking was performed using the Auto Dock Vina program.[26] The three dimensional crystal structures of BSA and HSA were downloaded from the RCSB Protein Data Bank in the pdb format. The water molecules surrounding BSA and HSA were removed and Kollman charges were added after merging all the non-polar hydrogen atoms. The coordinate file of BSA and HSA was then saved into PDBQT. The size of the grid was

set to 80 × 60 × 86 Å with a maximum spacing of 1 Å to cover all the active sites in BSA and HSA with the center of the grid at x = 29.535, y = 31.826 and z = 23.5. The structure of oligomers was converted to the pdb format and post-modelling analysis was done using Discovery Studio 2016 and PyMol. The docked conformation with the lowest energy was selected for analysis.[25,26]

Results and discussion

The conducting polymers synthesized *via* interfacial polymerization are reported to show solubility in different solvents and dispensability in water as shown in Table S1 (ESI†) (provided in the ESI†).[21,22] WD-PTh and WD-PPy showed a uniform morphology as discussed in SEM in the proceeding section. The interaction between the organic solvents used in interfacial polymerization plays an important role in enhancing the miscibility of WD-PPy and WD-PTh in water as the monomer is soluble in the organic solvent while the initiator (ferric chloride) is soluble in the water medium. It has been reported that $FeCl_3$ exhibits good solubility in organic solvents as well as water and can lower the oxidation potential of thiophene to accelerate polymerization and likely form an oligomer. Hence it can be concluded that interfacial polymerization in our case leads to the formation of oligomers of WD-PTh and WD-PPy due to which they show dispersibility in water.

Morphological studies

The SEM image of WD-PPy, Fig. 1(a), exhibited a granular morphology and the particles appeared to be scattered as tiny grains. The SEM of WD-PTh, Fig. 1(b), showed bright dense spherical clusters. The SEM of WD-PPy/PTh-4/1, Fig. 1(c), showed the predominance of the PPy morphology (loading was higher) with the appearance of bright PTh particles as agglomerates. The SEM of WD-PPy/PTh-1/1, Fig. 1(d), showed a granular morphology with a uniform distribution of PPy/PTh particles that appeared to be well-interconnected. The SEM of WD-PPy/PTh-1/4, Fig. 1(e), revealed flaky particles of PTh forming dense granular agglomerates. The predominance of WD-PPy showing a dull granular morphology was noticed in WD-PPy/PTh-4/1, while the predominance of the WD-PTh morphology showing bright clusters of white particles was observed in WD-PPy/PTh-1/4. A mixed morphology was noticed in WD-PPy/PTh-1/1. The SEM studies clearly reflected the variation in the morphology upon loading of PPy and PTh at various concentrations.

Confirmation of polymer structures *via* ^{1}H-NMR and IR studies

The ^{1}H-NMR spectrum of WD-PPy (given in the ESI† as Fig. S1(a)), revealed a sharp peak at δ = 8.3 ppm of NH protons of pyrrole.[24] The heterocyclic ring protons adjacent to the NH group appeared at δ = 7.3 ppm and δ = 7.6 ppm. The ^{1}H-NMR spectrum of WD-PTh (given in the ESI† as S1(b)) exhibited a doublet peak at δ = 7.2 ppm and δ = 7.4 ppm corresponding

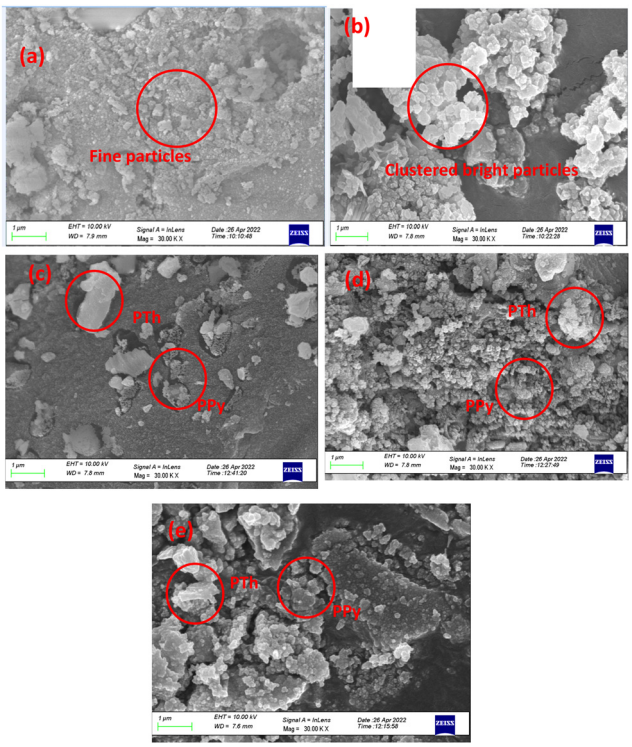

Fig. 1 SEM of (a) WD-PPy, (b) WD-PTh, (c) WD-PPy/PTh-4/1, (d) WD-PPy/PTh-1/1, and (e) WD-PPy/PTh-1/4.

to the protons of the heterocyclic ring of PTh. The ^{1}H-NMR spectrum of WD-PPy/PTh-1/1 (given in the ESI† as S1(c)) showed 2 broad humps at δ = 6.8 ppm and δ = 7.9 ppm correlated with the heterocyclic ring protons of PPy/PTh and the NH proton of the pyrrole ring, respectively. The peaks appeared to be broad and diffused due to the incorporation of PTh in PPy and *vice versa*. The broadness of the humps was even related to hydrogen bonding with the solvent (DMSO). The ^{13}C-NMR spectrum of WD-PPy (given in the ESI† as Fig. S2(a)), revealed a sharp peak at δ = 112 ppm corresponding to protonated carbons in the pyrrole ring (b).[25–27] The peak at around 128 ppm was correlated with the protonated carbon (a) adjacent to the NH group, while the peak at 117 ppm was correlated with unprotonated carbons (c).[27] The ^{13}C-NMR spectrum of WD-PTh (given in the ESI† as S2(b)) exhibited peaks at δ = 113 ppm and δ = 117 ppm corresponding to the protonated carbons and unprotonated carbons of the heterocyclic ring of PTh respectively.[28] The peak at 129 ppm was associated with the unprotonated carbons adjacent to the S group of thiophene. The ^{13}C-NMR spectrum of WD-PPy/PTh-1/1 (given in the ESI† as S1(c)) showed peaks at δ = 109 ppm, 117 ppm, 128 ppm, and 130 ppm correlated with the protonated carbons of WD-PPy and WD-PTh, respectively.[29] The peaks of the homo-oligomers showed a slight shift indicating the formation of block copolymers as shown in Scheme 1. For alternate copolymers several peaks would have appeared in the spectrum due to alternate linkages but the neatness, as well as the appearance of the peaks corresponding to homooligomers, clearly reveals the formation of a block copolymer as shown in Scheme 1.

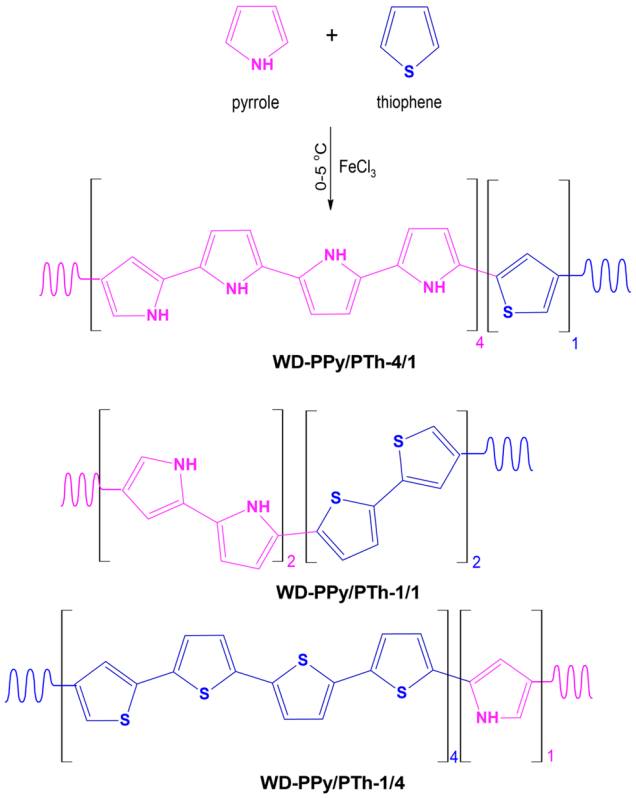

Scheme 1 Copolymerization of WD-PPy with WD-PTh.

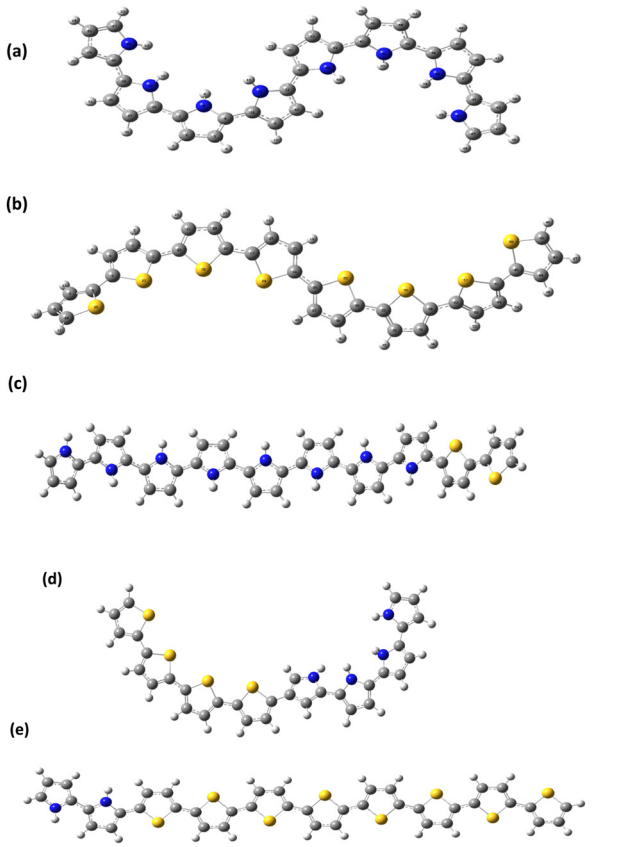

Fig. 2 Optimized geometries of (a) WD-PPy,(b)WD-PTh, (c) WD-PPy/PTh-4/1, (d) WD-PPy/PTh-1/1, and (e) WD-PPy/PTh-1/4.

Based on the synthesis technique we have used, it is very unlikely that an alternate copolymer can be formed. The reactivity ratios of pyrrole and thiophene show the tendency to homo-polymerize and form short chains which subsequently react with the other monomers or oligomeric chains to form copolymers. The chemical oxidant polymerization utlilizes

Table 1 IR spectral data of WD-PPy, WD-PTh, WD-PPy/PTh-4/1 WD-PPy/PTh-1/1 and WD-PPy/PTh-1/4

		Peak position (cm^{-1})	
Polymer	Functional group	Experimental	Theoretical
WD-PPy	NH deformation	3488	3616, 3476
	C═N stretching	1605, 1045	1588, 1048
	C═C stretching	1441, 1409, 1323	1450, 1408, 1343
	C–C stretching	1211, 1142, 1018	1210, 1140, 1020
	Pyrrole ring	842, 760, 699	840, 768, 688
WD-PTh	OH stretching	3424	3445, 3250
	C═C stretching	1523, 1424, 1409, 1323	1524, 1430, 1400, 1320
	C–S–C stretching	1021, 1019	1130, 1010
	thiophene ring	952, 908, 701	955, 918, 705
WD-PPy/PTh-4/1	OH/NH	3438	3622, 3459
	C═N stretching	1566, 1435, 1409	1564, 1430, 1397
	C═C stretching	1402, 1285, 1021	1408, 1282, 1025
	C–S–C stretching	1134, 1095	1138, 1093
	Pyrrole/thiophene ring	952, 904, 744, 680	950, 909, 777, 675
WD-PPy/PTh-1/1	OH/NH	3417	3620, 3422
	C═N stretching	1566, 1435, 1017	1565, 1432, 1018
	C═C stretching	1361, 1224	1371, 1248
	C–S–C stretching	1142, 1013	1138, 1018
	Pyrrole/thiophene ring	951, 754, 698	958, 747, 710
WD-PPy/PTh-1/4	OH/NH	3415	3650, 3244
	C═N stretching	1578, 1435, 1019	1570, 1430, 1015
	C═C stretching	1409, 1354, 1316	1408, 1355, 1317
	C–S–C stretching	1252	1255
	Pyrrole/thiophene ring	974, 905, 804, 745, 700	976, 908, 800, 740, 655

a strong oxidant which leads to quick radical generation in monomers and fast polymerization forming oligomers instantly. As far as computational studies are concerned, we tried correlating the experimental FTIR and UV visible studies with the theoretical data generated by combining alternate and random sequences. The theoretical IR and UV-visible results did not match our experimental data except in the case of the block sequence that we used. The theoretical and experimental FTIR studies were carried out to confirm the geometry-optimized structures utilized for determining the band gap and electronic transitions. The FT-IR spectrum of WD-PPy (provided in the ESI† as Fig. S3(a)), Table 1, showed absorption peaks at 3488 cm^{-1} corresponding to NH deformation. The theoretical spectrum displayed the same peaks at 3616 and 3476 cm^{-1}. The peaks at 1605 cm^{-1} and 1045 cm^{-1} were correlated with the C=N stretching and those at 1588 cm^{-1} and 1048 cm^{-1} were observed in the theoretical spectrum of PPy. The C=C stretching peaks were observed at 1441 cm^{-1}, 1409 cm^{-1} and 1323 cm^{-1}, while the theoretical spectrum showed the same peaks at 1450 cm^{-1}, 1408 cm^{-1}, and 1343 cm^{-1}. The C–C stretching vibration peak appeared at 1211 cm^{-1}, 1142 cm^{-1}, and 1018 cm^{-1}, while the peaks at 842 cm^{-1}, 760 cm^{-1}, and 699 cm^{-1} were associated with pyrrole ring deformations. The theoretical spectrum revealed these peaks at 1210 cm^{-1}, 1140 cm^{-1}, 1020 cm^{-1}, 840 cm^{-1}, 768 cm^{-1}, and 688 cm^{-1} respectively. The peaks confirmed the polymerization of pyrrole as reported by other authors.[29]

The IR spectrum of WD-PTh (provided in the ESI† as Fig. S3(b)), Table 1, showed the OH stretching vibration at 3424 cm^{-1}, while the theoretical spectrum revealed the same vibrations at 3445 cm^{-1} and 3250 cm^{-1}. The C=C stretching vibration peaks were observed at 1523 cm^{-1}, 1424 cm^{-1}, 1409 cm^{-1}, and 1323 cm^{-1} and the theoretical spectrum showed the same peaks at 1524 cm^{-1}, 1430 cm^{-1}, 1400 cm^{-1}, and 1320 cm^{-1}. The C–S–C stretching peaks appeared at 1021 cm^{-1} and 1019 cm^{-1} in the experimental spectrum and at 1130 cm^{-1} and 1010 cm^{-1} in the

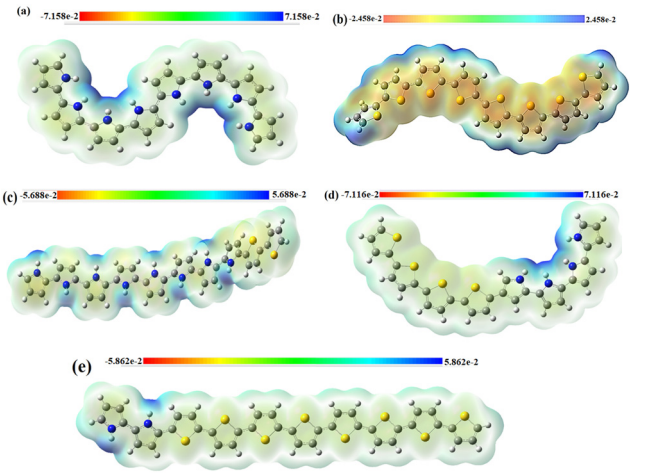

Fig. 4 MEP of (a) WD-PPy, (b) WD-PTh, (c) WD-PPy/PTh-4/1, (d) WD-PPy/PTh-1/1, and (e) WD-PPy/PTh-1/4.

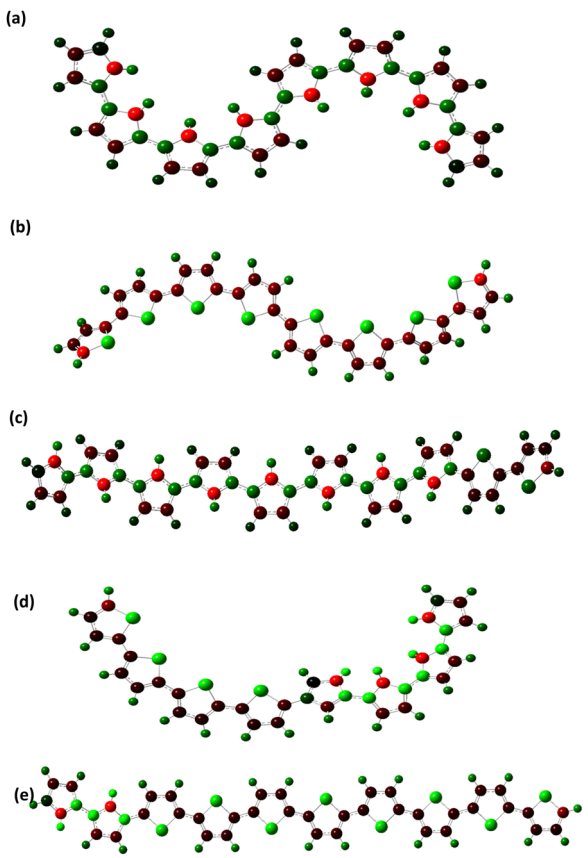

Fig. 3 Mulliken charge distribution in (a) WD-PPy,(b)WD-PTh, (c) WD-PPy/PTh-4/1, (d) WD-PPy/PTh-1/1, and (e) WD-PPy/PTh-1/4.

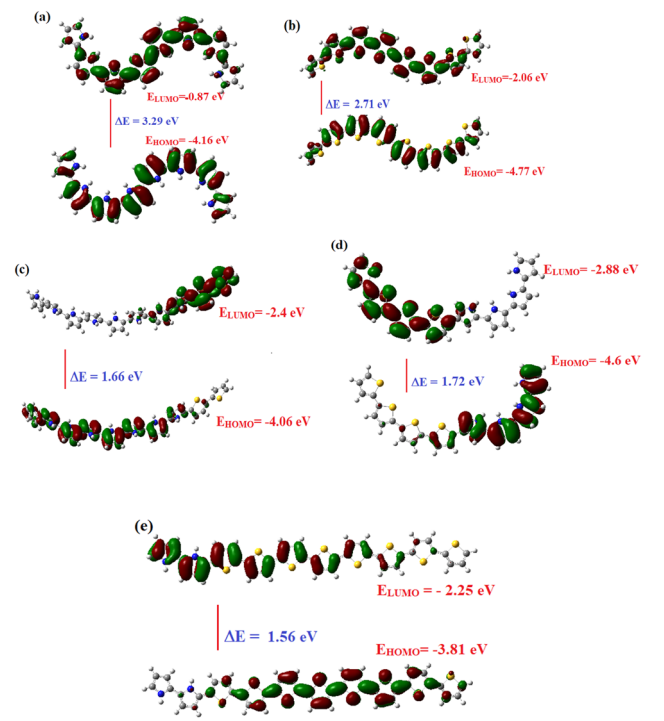

Fig. 5 HOMO–LUMO distributions in (a) WD-PPy, (b) WD-PTh, (c) WD-PPy/PTh-4/1, (d) WD-PPy/PTh-1/1, and (e) WD-PPy/PTh-1/4.

theoretical spectrum. The peaks at 952 cm^{-1}, 908 cm^{-1}, and 701, cm^{-1} correlated with the presence of a thiophene ring and confirmed the occurrence of polymerization.[19,29]

The IR spectrum of WD-PPy/PTh-4/1 (provided in ESI† as Fig. S3(c)), Table 1, showed the NH stretching vibration at 3438 cm^{-1} in the experimental spectrum and at 3622 cm^{-1} and 3459 cm^{-1} in the theoretical spectrum, respectively. The C═N stretching peaks were noticed at 1566 cm^{-1}, 1435 cm^{-1} and 1017 cm^{-1} in the experimental spectrum and at 1564 cm^{-1}, 1430 cm^{-1} and 1397 cm^{-1} in the theoretical spectrum. The C═C stretching peaks appeared at 1402 cm^{-1}, 1285 cm^{-1}, and 1021 cm^{-1} and the C–S–C stretching vibrations were observed at 1408 cm^{-1}, 1282 cm^{-1} and 1205 cm^{-1} while the heterocyclic ring vibrations were seen at 952 cm^{-1}, 904 cm^{-1}, 744 cm^{-1}, and 680 cm^{-1}. The theoretical spectrum was found to be in close agreement with the experimental spectrum. The IR spectrum of WD-PPy/PTh-1/1 (provided in the ESI† as Fig. S3(d)), Table 1, showed the NH stretching vibration at 3417 cm^{-1}. The C═N stretching peaks were found at 1566 cm^{-1}, 1435 cm^{-1} and 1017 cm^{-1}. The C═C stretching peaks appeared at 1361 cm^{-1} and 1224 cm^{-1} and the C–S–C stretching peaks were noticed at 1142 cm^{-1}, and 1013 cm^{-1}. The heterocyclic ring vibrations were observed at 951, cm^{-1}, 754 cm^{-1}, and 698 cm^{-1}, respectively. Likewise, the IR spectrum of WD-PPy/PTh-1/4 (provided in the ESI† as Fig. S3(e)), Table 1, exhibited the NH stretching vibration peak at 3415 cm^{-1} and the C═N stretching vibration peaks appeared at 1578 cm^{-1}, 1435 cm^{-1}, and 1019 cm^{-1}, while the C═C stretching peaks were found at 1409 cm^{-1}, 1354 cm^{-1}, and 1316 cm^{-1}. The C–S–C stretching vibration peaks appeared at 1252 cm^{-1}. The theoretical spectrum also revealed the same peaks with a minor shift and the presence of the peaks associated with WD-PPy and WD-PTh confirmed the occurrence of polymerization. The experimental spectra in all cases were found to be in close agreement with the theoretical spectra.

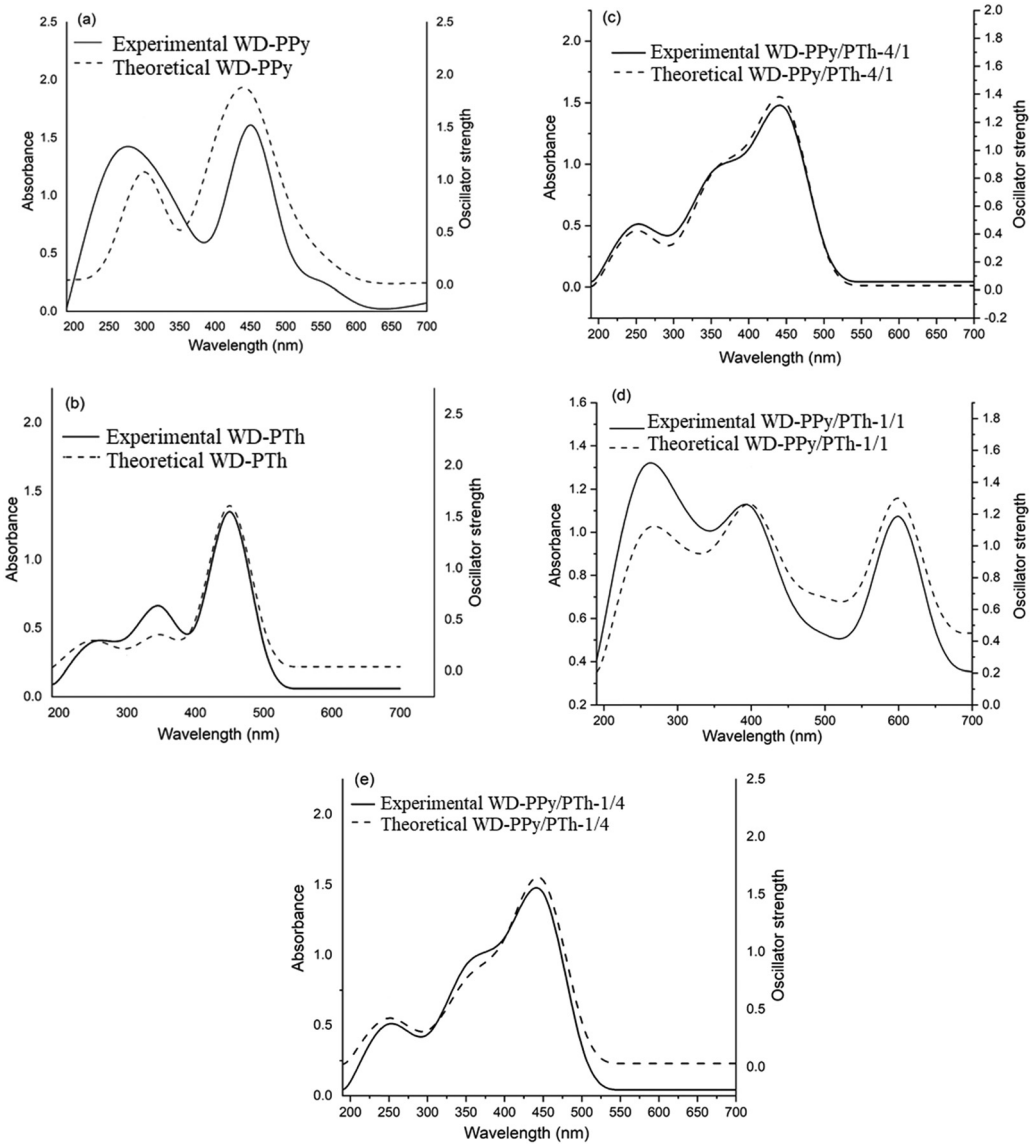

Fig. 6 UV-visible spectra of (a) WD-PPy, (b) WD-PTh, (c) WD-PPy/PTh-4/1, (d) WD-PPy/PTh-1/1, and € Wd-PPy/PTh-1/4.

DFT studies: muliken charge distribution and frontier molecular orbitals

The geometry optimized structures of WD-PPy, WD-PTh, WD-PPy/PTh-4/1, WD-PPy/PTh-1/1, and WD-PPy/PTh-1/4 are depicted in Fig. 2(a–e). The geometries were optimized taking 8 units of the pyrrole ring and thiophene ring for WD-PPy and WD-PTh, respectively. For the co-oligomers, the ratios were taken to be 2 units of the thiophene ring and 8 units of the pyrrole ring for WD-PPy/PTh-4/1, 4 units of the thiophene ring and 4 units of the pyrrole ring for WD-PPy/PTh-1/1 and 8 units of the thiophene ring and 2 units of the pyrrole ring for WD-PPy/PTh-1/4. This optimization was chosen based on our DFT calculations of alternating-like, random, as well as block sequences with PPy

and PTh that could match with the experimental studies. Only block structures were used in the model as they were in close agreement with the experimental data. The rest of the calculations did not match the experimental results. For WD-PPy, Fig. 2(a), the C–C and C=C bond lengths were computed to be 1.42 Å and 1.39 Å. The N–H bond length was computed to be 1.007 Å and the C–N bond length was found to be 1.39 Å. Similarly, for WD-PTh, Fig. 2(b), the C–C bond length was found to be 1.44 Å, and the C=C bond was calculated to be 1.38 Å, while the C–S bond length was computed to be 1.75 Å. The geometry optimized structure of WD-PPy/PTh-4/1, Fig. 2(c), showed C–C and C=C bond lengths to be 1.44 Å and 1.39 Å, respectively, while the NH bond length was computed to be 1.008 Å. The C–N and C–S bond lengths were computed to be 1.38 Å and 1.75 Å, respectively. The geometry optimized structure of WD-PPy/PTh-1/1, Fig. 2(d) and (e), revealed the bond lengths to be similar to the previous co-oligomer. The pristine WD-PPy and WD-PTh showed twisting of the chains but upon insertion of thiophene/pyrrole, the structures attained a planar configuration, Fig. 2(c)–(e).

Mulliken charge distribution

The charge distribution in WD-PPy, Fig. 3(a) was concentrated on nitrogen atoms of the pyrrole ring, and for WD-PTh, Fig. 3(b), it was noticed to be concentrated over the terminal carbon atoms of the thiophene ring. For WD-PPy/PTh-4/1, WD-PPy/PTh-1/1, and WD-PPy/PTh-1/4, the charge distribution was similar to the parent oligomer and did not show any significant change upon co-oligomerization.

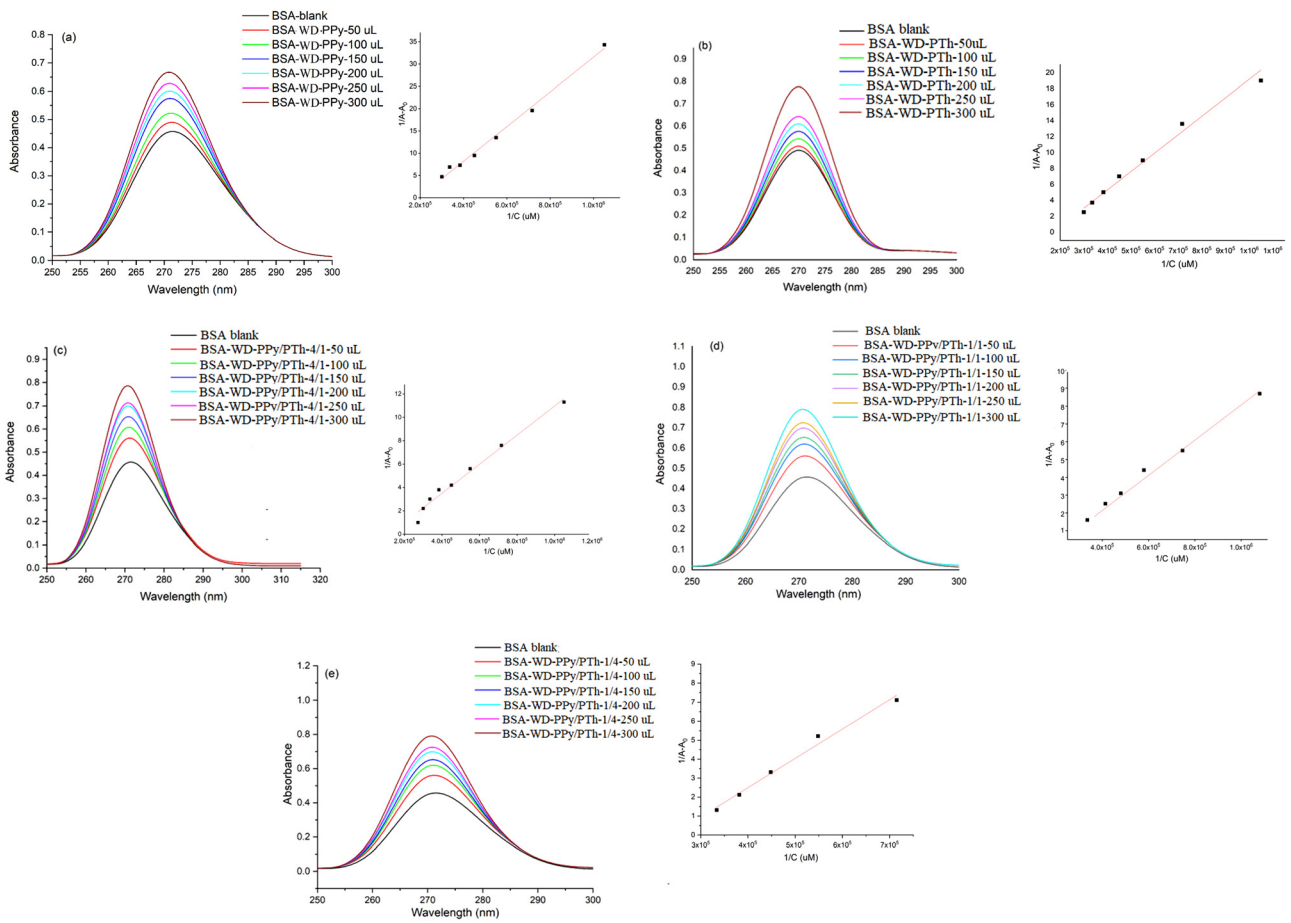

Fig. 7 UV–vis absorption spectra of BSA in (a) WD-PPy, (b)WD-PTh,(c) WD-PPy/PTh-4/1, (d) WD-PPy/PTh-1/1, and (e) WD-PPy/PTh-1/4 (inset plot of $1/(A - A_0)$ *vs.* $1/[C]$).

Molecular electrostatic potential (MEP)

The molecular electrostatic potential (MEP) is depicted in Fig. 4(a–e). For WD-PPy, Fig. 4(a), the MEP is noticed to be blue around the NH bonds indicating the maximum electrostatic potential. Similarly, for WD-PTh, Fig. 4(b), the MEP was noticed to be in the yellow region indicating a lower electrostatic potential. Interestingly, for WD-PPy/PTh-4/1, WD-PPy/PTh-1/1 and WD-PPy/PTh-1/4, Fig. 4(c)–(e), the MEP was noticed to be intermediate of the pristine polymers. The electrostatic potential can help predict chemical reactivity as regions of negative potential are sites of protonation and nucleophilic attack, while regions of positive potential indicate electrophilic sites. In our case the co-oligomers show sites of protonation and nucleophilic attack. The highest occupied molecular orbital (HOMO) and lowest unoccupied molecular orbital (LUMO) were noticed to be uniformly delocalized in the case of WD-PPy, Fig. 5(a). The band gap was calculated to be 3.29 eV. The HOMO–LUMO orbitals were found to be uniformly distributed in WD-PTh as well and the band gap in this case was computed to be 2.71 eV, Fig. 5(b). For WD-PPy/PTh-4/1, Fig. 5(c), the band gap was computed to be 1.66 eV. The LUMO orbitals were noticed to be concentrated around the thiophene rings and the pyrrole units were attached to the thiophene rings, while the HOMO orbitals were uniformly delocalized throughout the structure. Likewise, for WD-PPy/PTh-1/1, Fig. 5(d), the LUMO orbitals were highly delocalized around the thiophene units and the HOMO orbitals were noticed to be concentrated around the pyrrole units. The band gap was found to be 1.72 eV which was found to be higher than in the previous case. The delocalized distribution of LUMO orbitals was noticed for WD-PPy/PTh-1/4, Fig. 5(e), while the HOMO orbitals were distributed over the thiophene units. The band gap was computed to be 1.56 eV.

Hence, it can be concluded that the band gap could be optimized to desirable values by the incorporation of required units of pyrrole/thiophene rings.

The UV–visible spectrum of WD-PPy, Fig. 6 (a), exhibited two intense peaks at 260 nm due to n–π* transitions and 450 nm due to π–π* transitions. The theoretical spectrum (given in the inset) revealed the n–π* transitions at 300 nm and the π–π*transitions were noticed at 430 nm.[29] The oscillator strength of the later peak was computed to be 1.8. The UV spectrum of WD-PTh, Fig. 6(b), revealed n–π* transitions at 250 nm (a shoulder) and 320 nm, while the π–π* transition peak was observed at

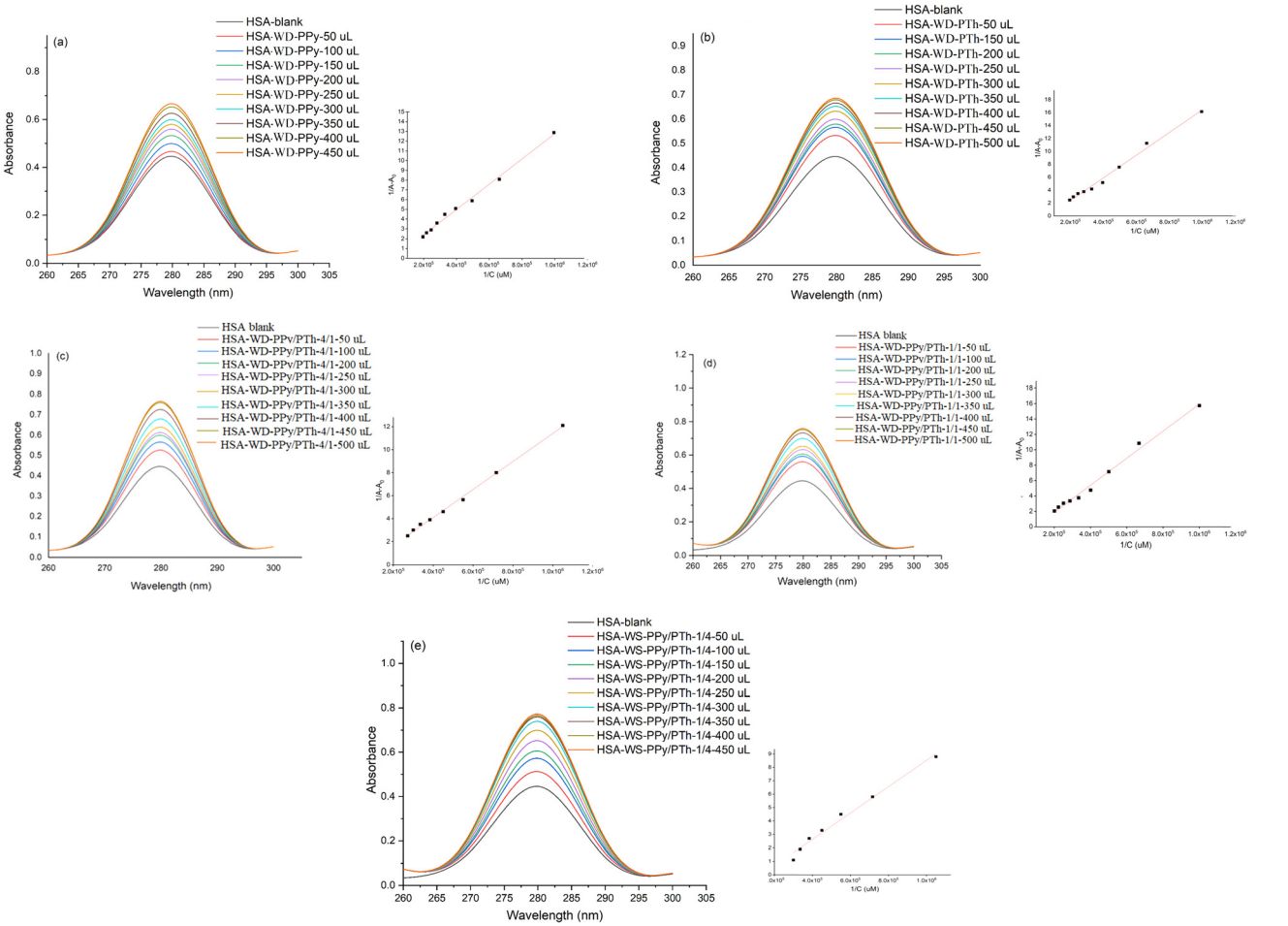

Fig. 8 UV–vis absorption spectra of HSA in (a) WD-PPy, (b)WD-PTh,(c) WD-PPy/PTh-4/1, (d) WD-PPy/PTh-1/1, and (e) WD-PPy/PTh-1/4 (inset plot of $1/(A - A_0)$ *vs.* $1/[C]$).

Table 2 Estimated binding constant (K_b) obtained using the Benesi-Hildebrand equation and binding energies obtained from docking results for WD-PPy/PTh-4/1, WD-PPy/PTh-1/1 and WD-PPy/PTh-1/4

Complexes	K_b (Benesi-Hildebrand equation) (μM^{-1})	Binding Energy (kcal mol^{-1})	List of amino acids involved in binding	Type of interactions	Distance (Å)
BSA interaction					
WD-PPy/PTh-4/1-BSA	5.2×10^5	−8.78	His18	Pi-cation	3.25
			Lys12	Pi-lone pair	2.89
			Leu282	Pi-alkyl	5.12
			Lys283	Pi-alkyl	4.94
			Lys159	Pi-alkyl	4.62
WD-PPy/PTh-1/1-BSA	7.4×10^5	−9.88	Ala193	Pi-Sigma	3.83
			Arg196	Pi–pi	4.90
			Arg435	Pi–pi	4.75
			Arg458	Pi-ionic	3.86
			Asp108	Pi-ionic	3.68
			Cys447	Pi–pi	5.27
			Glu186	Pi-ionic	4.77
			His145	Hydrogen bond	3.87
			Ile455	Pi–pi	5.33
			Lys431	Pi–pi	5.41
			Lys439	Pi-ionic	3.90
			Pro146	Pi–pi	4.99
			Tyr451	Hydrogen bond	2.49
WD-PPy/PTh-1/4-BSA	4.6×10^5	−8.34	Arg81	Pi-ionic	4.62
			Arg98	Pi-ionic	4.36
			Asp72	Hydrogen bond	2.27
			Cys75	Hydrogen bond	2.28
			Cys91	Hydrogen bond	4.50
			Glu95	Hydrogen bond	2.73
			Pro96	Pi-alkyl	5.06
			Thr68	Hydrogen bond	2.41
HSA interaction					
WD-PPy/PTh-4/1-has	8.3×10^5	−8.55	Ala213	Pi-Sigma	3.72
			Ala350	Pi-Sigma	4.97
			Arg209	Hydrogen bond	3.06
			Asp324	Hydrogen bond	2.61
			Glu354	Pi-ionic	4.81
			Leu327	Pi-Sigma	5.21
			Leu331	Pi-Sigma	5.44
			Lys205	Pi-ionic	3.70
			Lys351	Pi-Sigma	4.43
			Phe206	Pi-Sigma	3.94
			Val482	Pi-Sigma	4.68
WD-PPy/PTh-1/1-has	5.4×10^5	−8.25	Ala213	Pi-Sigma	4.54
			Ala350	Pi-alkyl	4.89
			Arg209	Pi-ionic	4.86
			Asp324	Hydrogen bond	2.48
			Leu327	Pi-alkyl	4.65
			Leu331	Pi-alkyl	5.13
			Leu347	Hydrogen bond	5.38
			Lys351	Pi-alkyl	4.52
			Phe206	Pi-ionic	5.32
			Val216	Pi-alkyl	4.98
			Val482	Pi-alkyl	4.85
WD-PPy/PTh-1/4-has	5.7×10^5	−8.48	Ala406	Pi-alkyl	4.03
			Ala552	Pi-alkyl	4.74
			Arg410	Pi-ionic	4.81
			Asp549	Pi-ionic	3.74
			Glu492	Pi-ionic	4.44
			Leu387	Pi-alkyl	3.86
			Lys402	Pi-alkyl	4.51
			Lys525	Hydrogen bond	4.89
			Lys538	Pi-Sigma	4.90
			Lys545	Pi-alkyl	5.25
			Met548	Pi-Sigma	4.89
			Ser489	Hydrogen bond	2.87
			Tyr401	Pi–pi	4.91
			Val 409	Pi-Sigma	5.22

450 nm.[19] The theoretical spectrum showed n–π* and π–π* transitions to be similar to the ones found in the experimental spectrum and the oscillator strength of the 450 nm peak was computed to be 1.7. The UV spectrum of WD-PPy/PTh-4/1,

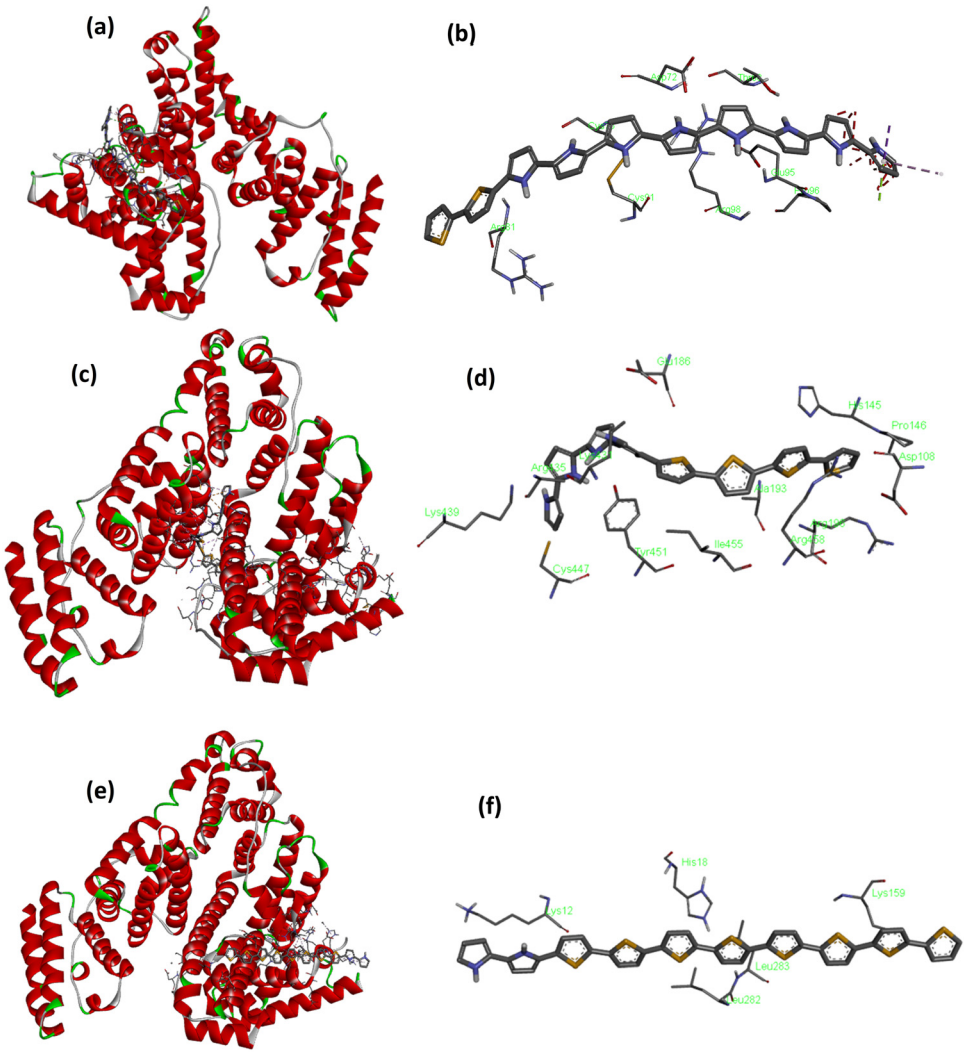

Fig. 9 Binding orientations of the lowest docking energy conformations of the oligomer-*co*-oligomer at site I of BSA: (a) WD-PPy/PTh-4/1-BSA complex, (b) amino acid residues for the WD-PPy/PTh-4/1-BSA complex zoomed in within 5 Å (3-D), (c) WD-PPy/PTh-1/1-BSA complex, (d) amino acid residues for the WD-PPy/PTh-1/1-BSA complex zoomed in within 5 Å (3-D), (e) WD-PPy/PTh-1/4-BSA complex, and (f) amino acid residues for the WD-PPy/PTh-1/4-BSA complex zoomed in within 5 Å (3-D).

Fig. 6(c), exhibited intense peaks at 250 nm, 360 nm, and 440 nm and the theoretical spectrum revealed similar peaks with the oscillator strength of peak at 440 nm to be 1.4. The UV spectrum of WD-PPy/PTh-1/1, Fig. 6(d), exhibited pronounced peaks at 250 nm, 400 nm, and 600 nm and the UV-spectrum of WD-PPy/PTh-1/4, Fig. 6(e) revealed an intense peak at 450 nm. The theoretical spectra showed transitions which were found to be in close agreement with the experimental spectra. The electronic transitions were found to vary with the number of pyrrole/thiophene units in the co-oligomers and the π–π^* transitions were noticeably prominent for a higher loading of pyrrole in WD-PPy/PTh-4/1.

Biophysical interaction studies

In this study, the UV–vis spectra of BSA and HSA were recorded at different concentrations of WD-PPy, WD-PTh, WD-PPy/PTh-4/1, WD-PPy/PTh-1/1, and WD-PPy/PTh-1/4 (50 uL – 300 uL for BSA and 50 μL – 500 μL for HSA) to investigate the binding of the macromolecules to the oligomers. The UV–vis absorption spectrum of BSA, Fig. 7(a), in the absence of an oligomer showed a prominent peak at 280 nm associated with the presence of aromatic amino acids. Likewise, the UV–vis absorption spectrum of HSA, Fig. 8 (a), showed a prominent peak at 275 nm associated with the presence of aromatic amino acids.

The titration of BSA and HSA with varying concentrations of WD-PPy, Fig. 7(a) and Fig. 8(a), led to the increase in absorbance thereby confirming the formation of the WD-PPy-BSA/HSA complex induced by binding.[30–32] The hydrophobicity of the microenvironment of the aromatic amino acid also revealed a decrease in residues due to the losing and unfolding of the protein skeleton. The titration of BSA and HSA with varying concentrations of WD-PTh, Fig. 7(b) and Fig. 8(b), also led to the increase in absorbance thereby confirming the formation of

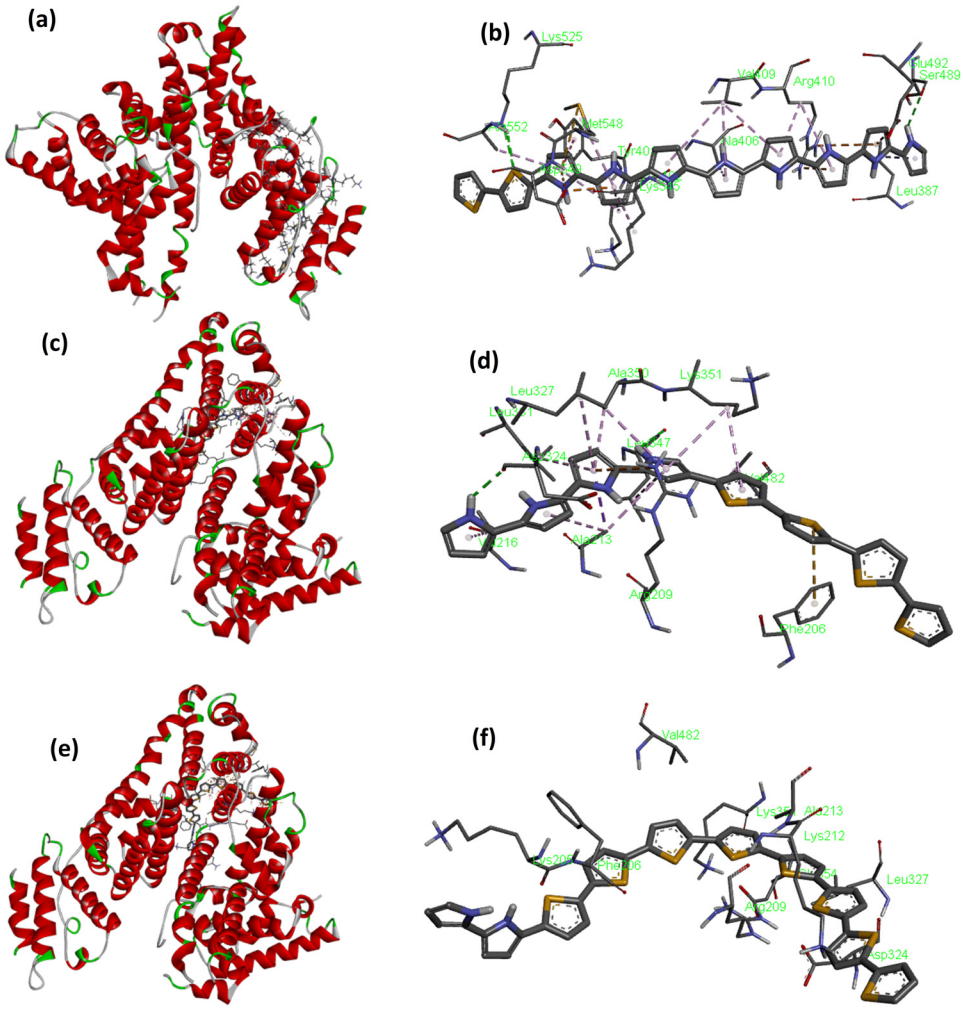

Fig. 10 Binding orientations of the lowest docking energy conformations of the oligomer-*co*-oligomer at site I of HSA: (a) WD-PPy/PTh-4/1-HSA complex, (b) amino acid residues for the WD-PPy/PTh-4/1-HSA complex zoomed in within 5 Å (3-D),(c) WD-PPy/PTh-1/1-HSA complex, (d) amino acid residues for the WD-PPy/PTh-1/1-HSA complex zoomed in within 5 Å (3-D), (e) WD-PPy/PTh-1/4-HSA complex, and (f) amino acid residues for the WD-PPy/PTh-1/4-HSA complex zoomed in within 5 Å (3-D).

the WD-PPy-BSA/HSA complex induced by binding. The titration of BSA and HSA with varying concentrations of WD-PPy/PTh-4/1, WD-PPy/PTh-1/1, and WD-PPy/PTh-1/4, Fig. 7(c)–(e) and Fig. 8(c)–(e) showed broadening of the peak corresponding to the BSA/HSA due to higher extent of unfolding of proteins. The binding constant value (K_b) was computed by taking λ_{max} = 275 nm for BSA and 280 nm for HSA, and was found to be 2.5×10^4 for WD-PPy with BSA, 7.7×10^4 for WD-PPy with HSA. The K_b values for WD-PTh with BSA and HSA were calculated to be 4.3×10^4 and 5.7×10^4, respectively. The K_b values for WD-PPy/PTh-4/1 with BSA were found to be an order higher indicating that the co-oligomers showed strong affinity for binding towards BSA and HSA, Table 2. The binding affinity was found to be higher for HSA than for BSA for all co-oligomers.

Docking studies

There are 3 types of interactions identified in the WD-PPy/PTh-4/1-BSA complex, Fig. 9(a) and (b) and Table 2. The pi-cation interaction with His18 balanced the N atom in the polymer. The other noticeable interactions are pi–alkyl interactions with Leu 282, Lys 283, and Lys 159 and the pi–lone pair interaction with Lys12. The binding energy was computed to be -8.78 kcal mol^{-1}. There were 2 hydrogen bond interactions noticeable in the WD-PPy/PTh-1/1-BSA complex, Fig. 9(c) and (d), Table 2, with His 145 and Tyr 45. The 6 pi–pi bond interactions were found with Arg196, Arg435, Cys 447, Ile 455, Lys 431 and Pro 146 while pi-ionic interactions were noticed for Arg458, Asp 108, Glu 186, and Lys 439, respectively. The binding energy was computed to be -9.88 kcal mol^{-1}. For the WD-PPy/PTh-1/4-BSA complex, Fig. 9(e) and (f), 5 hydrogen bond interactions were noticeable with Asp72, Cys 75, Cys 91, Glu 95 and Thr 68, while 2 pi–ionic interactions were present at Arg 81 and Arg98. The binding energy was computed to be -8.34 kcal mol^{-1}. The docking results of HSA complexes with WD-PPy/PTh are depicted in Fig. 10(a–e), Table 2. The WD-PPy/PTh-4/1-HSA complex, Fig. 10(a) and (b) revealed 7 pi-Sigma interactions with Ala 213, Ala 350, Leu 327, Leu 331, Lys 351, Phe206 and Val 482 amino acids. Hydrogen bond interactions were

prominent for Arg209 and Asp324, while pi–ionic interactions were notable for Glu 354, Table 2. The docking results for the WD-PPy/PTh-1/1-HSA complex, Fig. 10(c) and (d) showed 5 pi-alkyl interactions with Ala 350, Leu 327, Leu 331, Lys 351, Val 216 and Val 482, while one pi-Sigma interaction was found at Ala 213. There were 2 hydrogen bond interactions present at Asp 324 and Leu 347 and one pi-ionic interaction at Arg209. Similarly, the WD-PPy/PTh-1/4-HSA complex, Fig. 10(e) and (f), revealed 5 pi-alkyl interactions at Ala406, Ala552, Leu387, Lys402 and Lys545 whereas Arg 410, Asp 549, and Glu 492 showed pi-ionic interactions. The amino acids Lys525 and Ser489 exhibited hydrogen bond interactions, while Lys538, Val 409 and Met548 showed pi-Sigma interactions. The molecular docking results confirmed that the hydrophobic interactions and the hydrogen bonding had significant contributions to the binding energies, and pi-interactions contributed to the stabilization of the binding structures.

Conclusions

Water dispersible PPy and PTh and their co-oligomers were successfully synthesized. SEM studies confirmed the predominance of the morphology having higher loading of PPy/PTh based on its loading. ^{13}C-NMR also confirmed co-oligomerization and the formation of the block copolymer as shown by the experimental and theoretical FTIR studies. The theoretical and experimental UV studies confirmed that the electronic transitions were found to vary with the pyrrole/thiophene content in the co-oligomers. The UV studies showed an increase in the intensities of BSA/HSA upon addition of PPy/PTh oligomers. The binding constant (K_b) value was computed to be 2.5×10^4 for WD-PPy with BSA, 7.7×10^4 for WD-PPy with HSA, 4.3×10^4 for WD-PTh with BSA and 5.7×10^4 for WD-PTh with HSA, respectively. The K_b values were found to be higher for HSA than for BSA for all the co-oligomers. The binding energy was calculated to be the highest for the WD-PPy/PTh-1/1-BSA complex which was -9.88 kcal mol^{-1} and -8.55 J mol^{-1} for WD-PPy/PTh-4/1-HSA. The structural understanding and binding modes are vital factors affecting the binding free energies and provided valuable insights which could be utilized for designing biosensors. The fluorescence studies of these oligomers are underway in our laboratory and will be published soon.

Author contributions

This manuscript was written with the contributions of all authors. All authors have given approval to the final version of the manuscript. Ufana Riaz conceptualized the work and analyzed the results while Aaliyah Farooq carried out the synthesis of oligomers, Nuzhat Nabi carried out the docking studies, Faith Nwanze carried out the protein interaction studies and Fei Yang helped with the interpretation of the protein interaction studies.

Conflicts of interest

The authors declare no conflict of interest.

Acknowledgements

The work was funded by the National Science Foundation (Award # 2122044), the NSF PREM for Hybrid Nanoscale Systems. The corresponding authors wish to acknowledge NSF PREM for providing financial support.

References

1 U. Riaz, N. Singh and S. Banoo, Theoretical Studies of Conducting Polymers: A Mini Review, *New J. Chem*, 2022, **46**(11), 4954–4973.
2 D. Tzankova, S. Vladimirova, L. Peikova and M. Georgieva, Synthesis of Pyrrole and Substituted Pyrroles, *J. Chem. Technol. Met.*, 2018, **3**(53), 451–463.
3 J. Zia, F. Fatima and U. A. Riaz, Comprehensive Review on the Photocatalytic Activity of Polythiophene-Based Nanocomposites against Degradation of Organic Pollutants, *Catal. Sci. Technol.*, 2021, **11**(20), 6630–6648.
4 S. Jadoun, L. Biswal and U. Riaz, Tuning the Optical Properties of Poly(o-Phenylenediamine-Co-Pyrrole) via Template Mediated Copolymerization, *Des. Monomers Polym.*, 2018, **21**(1), 75–81.
5 S. Jadoun, A. Verma, S. M. Ashraf and U. Riaz, A Short Review on the Synthesis, Characterization, and Application Studies of Poly(1-Naphthylamine): A Seldom Explored Polyaniline Derivative, *Colloid Polym. Sci.*, 2017, **295**(9), 1443–1453.
6 B. Gupta and R. Prakash, Interfacial Polymerization of Carbazole: Morphology Controlled Synthesis, *Synth. Met.*, 2010, **160**(5), 523–528.
7 P. Mohankumar, J. Ajayan, T. Mohanraj and R. Yasodharan, Recent Developments in Biosensors for Healthcare and Biomedical Applications: A Review, *Measurement*, 2021, **167**, 108293.
8 P. Naskar, A. Maiti, P. Chakraborty, D. Kundu, B. Biswas and A. Banerjee, Chemical Supercapacitors: A Review Focusing on Metallic Compounds and Conducting Polymers, *J. Mater. Chem. A*, 2021, **9**(4), 1970–2017.
9 J. Gao, C. Wang, D.-W. Han and D.-M. Shin, Single-Ion Conducting Polymer Electrolytes as a Key Jigsaw Piece for next-Generation Battery Applications, *Chem. Sci.*, 2021, **12**(40), 13248–13272.
10 J. Zia and U. Riaz, Photocatalytic Degradation of Water Pollutants Using Conducting Polymer-Based Nanohybrids: A Review on Recent Trends and Future Prospects, *J. Mol. Liq.*, 2021, **340**, 117162.
11 R. Agrahari, B. Bayar, H. N. Abubackar, B. S. Giri, E. R. Rene and R. Rani, Advances in the Development of Electrode Materials for Improving the Reactor Kinetics in Microbial Fuel Cells, *Chemosphere*, 2022, **290**, 133184.
12 K. Tari, S. Khamoushian, T. Madrakian, A. Afkhami, M. J. Łos, A. Ghoorchian, M. R. Samarghandi and S. Ghavami, Controlled Transdermal Iontophoresis of Insulin from Water-Soluble Polypyrrole Nanoparticles: An In Vitro Study, *Int. J. Mol. Sci.*, 2021, **22**(22), 12479.

13 U. Haldar, S. Mondal, S. Hazra, S. Guin, L. Yeasmin, D. P. Chatterjee and A. Nandi, K. Tailor Made Synthesis of Water-Soluble Polythiophene-Graft-Poly(Caprolactone-Block-Dimethyl amino ethyl Methacrylate) Copolymer and Their PH Tunable Self-Assembly and Optoelectronic Properties, *Eur. Polym. J.*, 2022, **168**, 111124.
14 J. Stejskal and P. Bober, Progress in Research and Applications of Conducting Polymers: Topical Issue, *Chem. Pap.*, 2021, **75**(10), 4979–4980.
15 G. Bánhegyi, *Introduction. In Conducting Polymers for Advanced Energy Applications*, CRC Press, Boca Raton, 2021; 1–27.
16 H. Masuda and K. Kaeriyanma, Electrochemical Polymerization of Pyrrole with Water-Soluble Polymeric Electrolyte, *Synth. Met.*, 1995, **69**(1–3), 513–514.
17 Y. Lu, G. Shi, C. Li and Y. Liang, Thin Polypyrrole Films Prepared by Chemical Oxidative Polymerization, *J. Appl. Polym. Sci.*, 1998, **70**(11), 2169–2172.
18 A. O. Patil, Y. Ikenoue, F. Wudl and A. J. Heeger, Water Soluble Conducting Polymers, *J. Am. Chem. Soc.*, 1987, **109**(6), 1858–1859.
19 F. Wang, M. Li, B. Wang, J. Zhang, Y. Cheng, L. Liu, F. Lv and S. Wang, Synthesis and Characterization of Water-Soluble Polythiophene Derivatives for Cell Imaging, *Sci. Rep.*, 2015, **5**(1), 7617.
20 S. B. Tolani, M. Craig, R. K. DeLong, K. Ghosh and A. K. Wanekaya, Towards Biosensors Based on Conducting Polymer Nanowires, *Anal. Bioanal. Chem.*, 2009, **393**(4), 1225–1231.
21 S. Xing and H. Zheng, Preparation of polyaniline nanofibers using the organic solution of aniline as seed, **https://www.e-polymers.org**, ISSN 1618-7229.
22 X.-G. Li, J. Li, Q.-K. Meng and M.-R. Huang, Interfacial Synthesis and Widely Controllable Conductivity of Polythiophene Microparticles, *J. Phys. Chem. B*, 2009, **113**, 9718–9727.
23 N. Singh, R. Ali, S. M. Ashraf, A. Rub and U. Riaz, Experimental and Computational Studies of Novel Sudan-I Dye Modified Conjugated Oligomers: Efficient $^1O_2$ Generation and Antileishmanial Characteristics, *Mater. Sci. Eng. B*, 2021, **265**, 114993.
24 U. Riaz, S. M. Ashraf, S. Jadoun, V. Budhiraja and P. Kumar, Spectroscopic and Biophysical Interaction Studies of Water-soluble Dye modified poly(o-phenylenediamine) for its Potential Application in BSA Detection and Bioimaging, *Sci. Rep.*, 2019, **9**, 8544.
25 A. Das and G. S. Kumar, Binding Studies of Aristololactam-β-D-Glucoside and Daunomycin to Human Serum Albumin, *RSC Adv.*, 2014, **4**(62), 33082–33090.
26 S. Yasmeen and Riyazuddeen, Exploring Thermodynamic Parameters and the Binding Energetic of Berberine Chloride to Bovine Serum Albumin (BSA): Spectroscopy, Isothermal Titration Calorimetry and Molecular Docking Techniques, *Thermochim. Acta*, 2017, **655**, 76–86.
27 M. Maruthapandi, A. P. Nagvenkar, I. Perelshtein and A. Gedanken, Carbon-Dot Initiated Synthesis of Polypyrrole and Polypyrrole@CuO Micro/Nanoparticles with Enhanced Antibacterial Activity, *ACS Appl. Polym. Mater.*, 2019, **1**(5), 1181–1186.
28 F. Martinez, G. Neculqueo and M. E. Veas, Synthesis of 3,3'''-dioctyltetrathiophene oligomer, *Bol. Soc. Chil. Quím.*, 2000, **45**, 1.
29 P. Phukan, R. Chetia, R. Boruah, S. Konwer and D. Sarma, Fabrication of Polypyrrole/Cu(ii) Nanocomposite through Liquid/Liquid Interfacial Polymerization: ANovel Catalyst for Synthesis of NH-1,2,3-Triazoles in PEG-400, *Mater. Adv*, 2021, **2**(21), 6996–7006.
30 A. Banu, R. H. Khan, M. T. A. Qashqoosha, Y. K. Manea, M. Furkan and S. Naqyi, Multi-spectroscopic and computational studies of interaction of bovine serum albumin, human serum albumin and bovine hemoglobin with bisacodyl, *J. Nol. Struct.*, 2022, **1249**, 131550.
31 F. Rostamnezhad and M. H. Fatemi, Comprehensive investigation of binding of some polycyclic aromatic hydrocarbons with bovine serum albumin: Spectroscopic and molecular docking studies, *Bioorg. Chem.*, 2022, **120**, 105656.
32 C. Xu, J. Gu, X. Ma, T. Dong and X. Meng, Investigation on the interaction of pyrene with bovine serum albumin using spectroscopic methods, Spectrochim, *Acta Part A: Mol. Biomol. Spectros.*, 2014, **125**(5), 391–395.